Acoustic micro/nanorobots in medicine

Murat Kaynak[1,2], Amit Dolev[1], and Mahmut Selman Sakar[1]

[1]Institute of Mechanical Engineering, Ecole Polytechnique Fédérale de Lausanne, Lausanne 1015, Switzerland

[2]Center for Engineering in Medicine and Surgery, Massachusetts General Hospital, Harvard Medical School, Boston MA 02114, USA

1. Introduction

Sound is a vibration that propagates as a mechanical pressure wave through biological tissues. The use of sound in medicine started a long time ago. Auscultation is the act of listening to sounds within the body for diagnostic purposes. Doctors have used stethoscopes to listen to internal sounds generated through the presence of disturbed flow, such as eddies and turbulence, by frictional rubs or other sources with high accelerations (e.g., cardiac valve opening) since the early 19th century. Sonography, the use of ultrasound (> 20 kHz) to produce images, is now regularly used to monitor the developing baby's health, guide interventional procedures such as biopsies, visualize blood flow through a vessel, and diagnose diseases associated with almost all organs including the heart (i.e., echocardiography), urinary tract, and kidneys. The speed of sound wave propagation—approximately 1.5 km/s in soft tissue—allows ultrasound to operate with millisecond temporal precision. Sonography generates images several centimeters into tissue with spatial precision on the order of a few millimeters. These favorable properties, along with its relatively low cost, high portability, and safety, have made sonography one of the most widely used technologies in clinical medicine.

Applications of acoustics, the interdisciplinary science of sound, not only empower the clinician with the capability to record diagnostic signals and see visually hidden pathologies, but also provide the opportunity to "operate" inside living systems. For medical imaging, ultrasound has a frequency range from about 1 to 15 MHz, whereas therapeutic applications typically use a frequency of ~1 MHz or less. Sound waves can be focused to concentrate energy in a small volume, analogous to focusing light with a magnifying glass. Focused ultrasound can penetrate deep into the body and deposit energy in various shapes and sizes, generating a wide range of mechanical and thermal effects that can be used for treatment. Some effects like tissue destruction are

permanent, while others such as neuromodulation are transitory and reversible. Thermal ablation has been the most widely explored clinical application of focused ultrasound. There are a variety of conditions that can be treated using this technology including tumors in the prostate, breast, and liver; brain disorders such as essential tremor and Parkinson's disease; and neuropathic pain associated with bone metastasis. The thermal ablation of tissue is conducted with high-intensity ultrasound at power levels usually exceeding 600 W cm^{-2}, whereas ultrasound imaging is performed at significantly lower levels (< 0.2 W cm^{-2}). The mechanical effects of focused ultrasound can also be used for the precise destruction of tissue. Histotripsy is based on the use of inertial cavitation, the nucleation, growth, and destruction of tiny air bubbles. At high enough acoustic intensities with short pulse duration, inertial cavitation releases a shockwave, with amplitudes exceeding 10,000 atmospheres depending on the bubble size, capable of destroying cell membranes and even liquefying or annihilating cells. The same properties that make ultrasound attractive for imaging make it appealing for neuromodulation, including the ability of sound waves to penetrate deep into tissues and achieve high spatiotemporal precision. Transcranial-focused ultrasound has become a new non-invasive mode of regional brain stimulation, that can be used to stimulate or suppress neural activity.

This chapter describes the acoustic forces acting on microscale structures submerged in physiological media. Microrobotics research aims to harness forces generated on acoustically excited structures to create injectable or ingestible medical devices that can be transported and operated remotely inside the body. Such mechanical devices are envisioned to be used for minimally invasive surgery, targeted drug delivery, and the collection of liquid or solid biopsy samples. This approach is fundamentally different from another application area of sound waves—ultrasound-powered implantable miniaturized electronic devices. In such devices, a piezoelectric crystal sits on the chip and converts ultrasound waves into electrical energy. Bypassing the electrical circuitry and directly using sound waves to do mechanical work leads to the creation of significantly smaller devices. Notably, without piezo crystals and accompanying metal traces, the whole device can be manufactured from biocompatible and soft materials. The devices can be made mobile and actuated to deform in 3D. These novel features open new avenues for the use of acoustic micro/nanorobots in biology and medicine.

The rest of the chapter is organized as follows. A brief theoretical background of acoustical forces is provided in Sections 2. It focuses on primary and secondary acoustic radiation forces along with acoustic streaming induced drag and thrust forces. In Section 3, we discuss acoustical manipulation methods, namely acoustic tweezers that can be utilized in medicine. In Section 4, we describe the state-of-the-art micro-nanorobotic devices. We critically discuss the design, fabrication, actuation, and applications of these robots. Furthermore, we review the current *in vivo* applications of acoustic microrobotic systems in Section 5. In the last Section, we discuss acoustic robots in medicine and share our perspective.

2. Theoretical background

2.1 Introduction to acoustics

In this section, we introduce a non-exhaustive derivation of linear acoustics equations. In the following section, we discuss nonlinear acoustic phenomena, which require considering additional terms in the governing equations. The objective is to familiarize the reader with the physics behind acoustic waves' propagation and wave-matter interactions. For a detailed derivation, the interested reader is referred to the relevant literature[1–4].

To describe a lossless sound propagation in a homogenous fluid we need three equations: a) mass conservation, b) momentum conservation, and c) thermodynamic state. The conservation of mass requires that for a fixed volume the mass flux through the surfaces equals the time rate of change of the volume's mass. The conservation law can be written using volume and surface integrals. Using Gauss's theorem, and since the obtained result is valid for arbitrary volumes, the mass conservation (or continuity) equation is

$$\frac{\partial \rho}{\partial t} + \nabla \cdot (\rho \mathbf{v}) = 0, \tag{1}$$

where t is the time, ρ is the mass density, $\mathbf{v}$ is the fluid velocity vector, and $\nabla\bullet$ is the divergence operator.

The conservation of momentum for a fluid is derived from the conservation law of classical continuum mechanics, which states that the total force exerted on a fluid particle equals its mass times the acceleration of its center of mass. In general, gravity should be considered, but it can be

neglected[1] when considering acoustic disturbances at frequencies higher than g/c_0, where g is the gravitational acceleration and c_0 is the speed of sound. For water, it equates to frequencies lower than 0.01 Hz. In the following derivation, the surface forces are assumed normal, implying negligible viscosity, and the conservation of momentum equation is

$$\rho \frac{D\mathbf{v}}{Dt} = -\nabla p, \quad \frac{D\mathbf{v}}{Dt} = \frac{\partial \mathbf{v}}{\partial t} + (\mathbf{v} \cdot \nabla \mathbf{v}), \tag{2}$$

where p is the pressure, and the operator D/Dt is the material derivative.

The thermodynamic state of the fluid can be described by some definite relation

$$p = p(\rho, s), \tag{3}$$

where s is the specific entropy. Sound is neither an adiabatic nor an isothermal process, but for most cases of interest, it can be considered adiabatic, which is the same as $Ds/Dt = 0$. Therefore, Eq.(3) can be simplified to

$$p = p(\rho, s_0), \tag{4}$$

where s_0 is a constant, representing the specific entropy throughout the medium.

Linear acoustics considers the disturbances as a small perturbation to the ambient state of the fluid, which can be described by its ambient values, p_0, ρ_0, and $\mathbf{v}_0$. Hence, the fluid state can be described as:

$$p = p_0 + p_1, \quad \rho = \rho_0 + \rho_1, \quad \mathbf{v} = \mathbf{v}_0 + \mathbf{v}_1. \tag{5}$$

Here, subscript 1 indicates a small linear perturbation to the state. If the medium, through which the sound propagates, is homogenous, it means that the ambient quantities are position independent, if in addition they are time-independent and $\mathbf{v}_0 = 0$, the medium is quiescent. This idealization is a sufficient approximation for the description of most acoustic phenomena. Substituting Eq.(5) into the previously derived equations where the medium is assumed homogenous and quiescent, and considering only first-order terms (zero-order terms equate to zero), the linear acoustic equations are

$$\frac{\partial \rho_1}{\partial t} + \rho_0 \nabla \cdot \mathbf{v}_1 = 0, \quad \rho_0 \frac{\partial \mathbf{v}_1}{\partial t} = -\nabla p_1, \quad p_1 = c_0^2 \rho_1, \quad c_0^2 = \left(\frac{\partial p}{\partial \rho} \right)_0. \tag{6}$$

Equations (6) can be combined to derive the wave equation, which takes the form

$$\nabla^2 p_1 - \frac{1}{c_0^2}\frac{\partial^2 p_1}{\partial t} = 0, \tag{7}$$

where, operator ∇^2 is the Laplacian, which is the divergence of the gradient.

In the idealized case described thus far, the particles are displaced in parallel to the direction of propagation of the acoustic wave; therefore, it is called a longitudinal wave. This contrasts with transverse waves, such as the wave propagating on a string, where the particles are displaced perpendicularly to the direction of propagation. In both cases, it is important to note that the perturbation traveling from the source is transferred by the wave, and not by the particles which are barely displaced locally[1,2,4]. Most acoustic waves spread out spherically from a source[1,4], but for simplicity, we begin with waves propagating in a single Cartesian direction – plane waves. These waves are useful in understanding many acoustic concepts and can be used for approximating acoustic phenomena far from the source (see Figure 1). Plane waves propagating in a single Cartesian direction s (i.e., $s = \mathbf{n} \bullet \mathbf{x}$, where $\mathbf{n}$ is a unit vector) do not disturb the medium in the perpendicular plane. Therefore, all the field variables change only along s. For example, $p_1 = p_1(s,t)$ thus its gradient, ∇p_1, has only one component. As a result, Eq.(7) can be simplified to the following 1D wave equation:

$$\frac{\partial^2 p_1}{\partial s^2} - \frac{1}{c^2}\frac{\partial^2 p_1}{\partial t^2} = 0. \tag{8}$$

The general solution of Eq.(8) is a superposition of two arbitrary functions $f(t - s/c_0)$ and $b(t + s/c_0)$, as follows

$$p_1 = f\left(t - s/c_0\right) + b\left(t + s/c_0\right). \tag{9}$$

In addition, for the velocity field component in the s direction, one obtains:

$$v_1 = \frac{1}{\rho_0 c_0}\left[f\left(t - s/c_0\right) - b\left(t + s/c_0\right)\right]. \tag{10}$$

Figure 1. Illustration of a spherical wave that resembles a planar wave far from the source.

It can be understood that f describes a forward traveling wave in the $+s$ direction, while b describes a backward traveling wave in the $-s$ direction, both with speed c_0. The factor, $\rho_0 c_0$, is called the characteristic impedance of the medium. For simplicity, one can assume a forward traveling wave (i.e., $b = 0$) in a medium that was at rest before $t = 0$ (i.e., $f = 0$ for $t < 0$), and is $p_A \sin(\omega t)$ afterward as shown in Figure 2. The sinusoidal waveform travels from the source and reaches the location s_0 after $t_0 = s_0/c_0$. Right before t_0, the particles have positive velocity in the direction of propagation as indicated by the red arrows. The wave compresses the fluid and, as a result, ρ_1 increases. Since the pressure is temporarily larger to the left of s_0, its gradient points in the negative direction and the particles are being accelerated in the opposite direction. These two processes continue until a maximum value is obtained for p_a, at $t = \pi/2\omega$. Later, the pressure and compression begin to decrease and reach the ambient values at the pressure node at $t = \pi/\omega$. The process is then reversed, and minimum values are obtained at $t = 3\pi/2\omega$ when the pressure is minimal. During the second half of the cycle, the pressure and density decrease below the ambient values leading to fluid rarefaction, where the particle velocity is in the opposite direction to that of the wave propagation. It is important to note that if the time integral of f is zero, the fluid particles remain at the same place after the transmission of the acoustic wave.

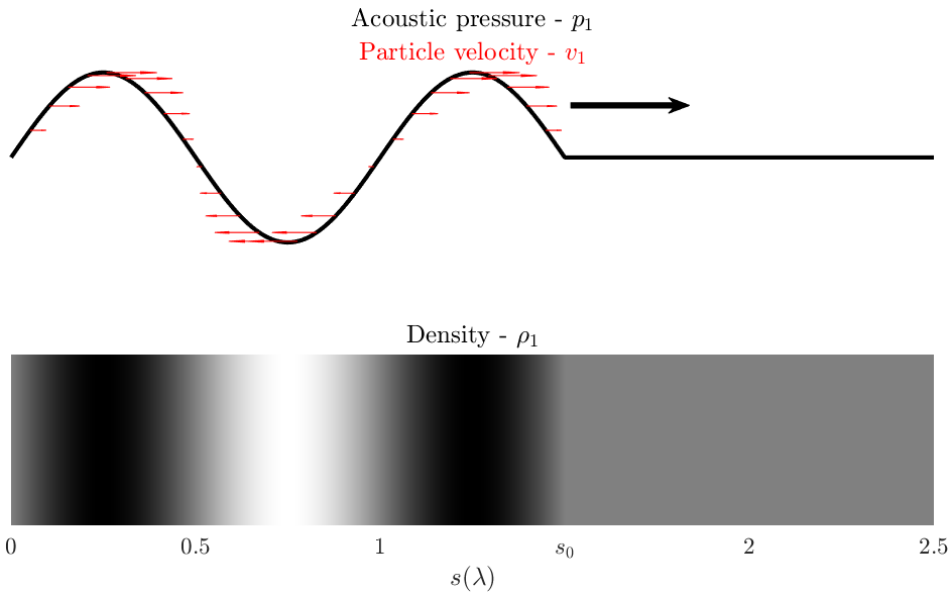

Figure 2. Sound wave propagation in a homogenous quiescent medium. Local and instantaneous pressure, particle velocity (Top), and density (Bottom) in the medium as the wave propagates.

Usually, when discussing acoustics, waves of constant frequencies are considered. At constant frequencies, the variables oscillate sinusoidally with time throughout the field. Therefore, at any point, the pressure can be described as follows,

$$p_1 = p_A \cos(\omega t - \varphi) = \mathrm{Re}\left\{\hat{p} \mathrm{e}^{-i\omega t}\right\}, \tag{11}$$

where p_A is the pressure amplitude, ω is the angular frequency, φ is the phase constant, $\hat{p}$ is the complex pressure amplitude, and Re denotes the real part. The complex pressure in Eq. (11) can be expressed as

$$\hat{p} = p_A \mathrm{e}^{i\varphi}, \quad \mathrm{e}^{i\varphi} = \cos(\varphi) + i\sin(\varphi). \tag{12}$$

For this kind of wave, there is a simple relation between the wave speed c_0, its frequency f, its wavelength λ, and the wavenumber k.

$$c_0 = \lambda f = \frac{\omega}{k}. \tag{13}$$

where the frequency f and the angular frequency ω are related as $\omega = 2\pi f$.

For a constant frequency, the time average of acoustical phenomena is computed as:

$$X_{\mathrm{av}} = \langle X \rangle = \frac{1}{T}\int_{t_0}^{t_0+T} X dt, \tag{14}$$

Here, X can be any quantity, the angled brackets represent the time-averaging operator, and T is either an integral number of wave periods or an infinite time integral. To compute the time average of a product of quantities oscillating at the same frequency, the complex notation leads to

$$\left(XY\right)_{\text{av}} = \left\langle XY \right\rangle = \frac{1}{2}\text{Re}\left\{\hat{X}\hat{Y}^{*}\right\}, \tag{15}$$

where the asterisk denotes the complex conjugate.

2.2 Time-averaged acoustically induced forces

Acoustically induced forces are associated with nonlinear phenomena occurring as the sound propagates through the medium and interact with the boundaries[1,3]. In Section 2.1, we neglected the fluid viscosity and higher-order terms that capture these phenomena to some extent. The full set of nonlinear equations capturing all the phenomena is very complex to analyze. In the following sections, specific terms are treated, focusing on primary and secondary acoustic radiation forces along with acoustic streaming.

a. Primary radiation forces

Bodies, deformable or rigid, are subjected to acoustic radiation pressure in an acoustic field due to the waves impinging their surface. Although we assume that the acoustic field is harmonic, a net force emerges, which is called *acoustic radiation force*. To compute the acoustic radiation force, time averaging is used along with the integration of the acoustic stress tensor $\boldsymbol{\sigma}$ over the surface. The elements of $\boldsymbol{\sigma}$ approximated to the second order are[3]:

$$\boldsymbol{\sigma} = \begin{pmatrix} -\left\langle p - p_0 \right\rangle - \rho_0 \left\langle v_{1x} v_{1x} \right\rangle & -\rho_0 \left\langle v_{1x} v_{1y} \right\rangle & -\rho_0 \left\langle v_{1x} v_{1z} \right\rangle \\ -\rho_0 \left\langle v_{1y} v_{1x} \right\rangle & -\left\langle p - p_0 \right\rangle - \rho_0 \left\langle v_{1y} v_{1y} \right\rangle & -\rho_0 \left\langle v_{1y} v_{1z} \right\rangle \\ -\rho_0 \left\langle v_{1z} v_{1x} \right\rangle & -\rho_0 \left\langle v_{1z} v_{1y} \right\rangle & -\left\langle p - p_0 \right\rangle - \rho_0 \left\langle v_{1z} v_{1z} \right\rangle \end{pmatrix}. \tag{16}$$

where v_{1x}, $v_{1y,}$ and v_{1z} are the Cartesian components of the first-order velocity field. In the idealized case of a rigid particle, the velocity on the surface nullifies, simplifying the stress tensor to

$$\sigma_{xx} = \sigma_{yy} = \sigma_{zz} = -\left\langle p - p_0 \right\rangle, \quad \sigma_{xy} = \sigma_{yx} = \sigma_{xz} = \sigma_{zx} = \sigma_{yz} = \sigma_{zy} = 0. \tag{17}$$

In the scope of this chapter, only small spherical particles are considered, where their radius R is much smaller than the acoustic wavelength λ and much larger than the viscous boundary layer $\delta = (\nu/\omega)^{½}$, where ν is the kinematic viscosity. The acoustic radiation force acting on an arbitrarily-

shaped body can be computed using numerical methods (e.g., finite element analysis) along with Eq.(16). For rigid and non-rigid spherical particles, there are analytical methods to calculate the acoustic radiation force. Solids and liquids in gasses can be idealized as rigid if they are much denser than the gas[3], King[5] computed analytically the acoustic radiation force acting on a rigid particle generated by plane incident standing waves and traveling waves. For the standing wave, where $p_1 = A\sin(kx)e^{-i\omega t}$, the resulting force is only in the x direction and is approximated as

$$F_{PRI}^{x} = -\frac{5\pi}{6}\frac{A^2 kR^3}{\rho_0 c_0^2}\sin(2kx). \tag{18}$$

Whereas for the traveling wave, where $p_1 = Ae^{[i(kx-\omega t)]}$, the force is approximated as

$$F_{PRI}^{x} = \frac{11\pi}{18}\frac{A^2 k^4 R^6}{\rho_0 c_0^2}. \tag{19}$$

In the former case, the force nullifies every quarter wavelength, which coincides with an equilibrium position. However, only pressure nodal points (i.e., $x = \lambda n/2$, $n \in \square$) are stable points to which the particle is attracted, and the anti-nodes (i.e., $x = \lambda(1+n/2)/4$, $n \in \square$) are unstable. In the latter case, the force is always positive, which means that the particle is pushed away from the source due to the momentum of the incident wave. Notably, the force produced by a standing wave is of order $(kR)^3$ times larger than the force produced by a traveling wave, since $kR<1$.

In the case of a compressible particle, such as a droplet or air bubble submerged in liquid, the compressibility, and density of the two media are comparable. Therefore, one can no longer assume a rigid sphere, and the velocity components in the acoustic radiation stress tensor must be considered. In the case of a gas bubble submerged in water, we can no longer assume that the frequency of the acoustic wave is much smaller than the sphere's resonance frequency. Yosioka and Kawasima[6] computed analytically the acoustic radiation force acting on a compressible sphere for incident plane standing and traveling waves. The resulting force for the standing wave is only in the x direction and is approximated as

$$F_{PRI}^{x} = \frac{\pi A^2 kR^3}{3}\left(\frac{1}{c_s^2\rho_s} + \frac{2\rho_0 - 5\rho_s}{c_0^2\rho_0(\rho_0 + 2\rho_s)}\right)\sin(2kx). \tag{20}$$

where ρ_s is the density of the particle and c_s is the speed of sound in the particle. The equilibrium points are analogous to the case of the rigid particle. However, the particle is attracted to either the

nodes or antinodes according to the particle and fluid properties (i.e., the term in the parenthesis can be positive or negative).

For an incident traveling wave the resulting force is approximated as

$$F_{PRI}^{x} = \frac{2\pi A^2 k^4 R^6 \rho_0}{c_0^2\left(\rho_0^2 + 2\rho_s^2\right)}\left(\frac{2\left(\rho_0 - \rho_s\right)^2}{9\rho_0^2} + \left(\frac{\rho_s}{\rho_0} - \frac{c_0^2\left(\rho_0 + 2\rho_s\right)}{3c_s^2\rho_s}\right)^2\right). \tag{21}$$

As for the rigid particle, the scaling of the forces and the force direction for a pure travelling wave are analogous.

In 1962, Gor'kov[7] derived a method to estimate the forces acting on a deformable small non-resonating particle. His method is valid for all cases, except for a pure travelling plane wave. To use his formula to calculate the acoustic radiation force, the values of the incident wave field variables (i.e., pressure p_1 and particle velocity $\mathbf{v}_1$) at a close neighborhood of the particle along with the physical properties of the surrounding medium and the particle must be measured. A potential field can be computed, whose gradient is the acoustic radiation force:

$$\mathbf{F} = -\nabla U, \quad U = 2\pi R^3\left[\frac{\rho_s c_s^2 - \rho_0 c_0^2}{2\rho_0 c_0^2 \rho_s c_s^2}\left\langle p_1^2\right\rangle - \frac{\rho_0\left(\rho_s - \rho_0\right)}{\rho_0 + 2\rho_s}\left\langle \mathbf{v}_1 \cdot \mathbf{v}_1\right\rangle\right]. \tag{22}$$

Similar to the results obtained by Yosioka and Kawasima for a compressible particle, the force changes sign according to the properties of the particle and fluid. A more elaborate model considering also thermal effects was developed by Karlsen and Bruss[8]. Calculating the acoustic radiation force acting on a gas bubble in a liquid requires further development since bubbles can resonate.[2] Here, the first vibration mode of a spherical bubble is considered, which is a volumetric vibration mode. At this vibration mode, the bubble experiences monopole oscillations. These volumetric oscillations are more important than the bubble's compressibility[3], and the force acting on it can be approximated as:[2,9]

$$\mathbf{F} \approx -\left\langle V\nabla p\right\rangle, \tag{23}$$

where V is the bubble's instantaneous volume. Since the bubble is subjected to an oscillating pressure field, either standing or traveling or a combination of thereof, its radius also oscillates as

$$R = R_0 + R_\varepsilon\left(t\right), \tag{24}$$

where R_0 is the bubble's radius at rest. Assuming small acoustic pressure amplitudes, the variations in the radius are also small compared to the equilibrium radius oscillations (i.e., $|R_\varepsilon| \ll R_0$). The linear radial oscillations equation of a bubble is[2,10,11]

$$\frac{\partial^2 R_\varepsilon}{\partial t^2} + \omega\delta\frac{\partial R_\varepsilon}{\partial t} + \omega_0^2 R_\varepsilon = -\frac{p_1(x,t)}{\rho_0 R_0}. \tag{25}$$

where ω is the acoustic field angular frequency, ω_0 is the bubble's natural frequency and δ is the total damping constant[9,11,12]. Assuming harmonic excitation, i.e., $\partial\bullet/\partial t = -i\omega$, the radial oscillations of the bubble are:

$$R_\varepsilon = \frac{p_1(x)}{\rho_0 R_0\left(\omega^2 - \omega_0^2 + i\omega^2\delta\right)}. \tag{26}$$

Substituting Eq.(26) into Eq.(23), and assuming that the pressure gradient can be estimated at the center of the bubble since $R_0 << \lambda$ we obtain for a traveling wave field:

$$F_{PRI}^x = \frac{2\pi A^2\delta R_0}{\rho_0\omega^2\left\{\left[1-(\omega_0/\omega)^2\right]^2 + \delta^2\right\}}, \tag{27}$$

and for a standing wave field:

$$F_{PRI}^x = -\frac{\pi A^2 R_0\left(1-(\omega_0/\omega)^2\right)}{\rho_0\omega^2\left\{\left[1-(\omega_0/\omega)^2\right]^2 + \delta^2\right\}}\sin(2kx). \tag{28}$$

The force is always positive in the traveling wave case, which means that the bubble is pushed away from the source.

The acoustic radiation force acting on a bubble in a standing wave field is often termed the *primary Bjerknes force*. Notice that if only the first natural frequency is considered, then the bubble oscillates in phase when $\omega_0 \ll \omega$ and out of phase when $\omega_0 \gg \omega$. To understand the behavior of a bubble when it is excited at different frequencies, one can write:

$$F_{PRI}^x \propto \begin{cases} \sin(2kx) & \omega_0 > \omega \\ -\sin(2kx) & \omega_0 < \omega \end{cases} \tag{29}$$

Equation (29) suggests that bubbles that are excited at a frequency below their natural frequency move toward pressure antinodes, while bubbles that are excited above their natural frequency move toward pressure nodes. Notice that Eq.(28) is singular when $\omega = \omega_0$, Yosioka, Kawashima,

and Hirano[3,13] derived a more complete model that is not singular with which Eq.(28) agrees. If higher vibration modes are considered, the bubble dynamics is more complex, and the interested reader is referred to a comprehensive treatment by Doinikov[9] for further details.

b. Secondary radiation forces

Particles excited by an incident pressure field apply *secondary acoustic radiation forces* on neighboring particles. These forces arise when compressible particles can resonate, which is particularly relevant for gas bubbles. Acoustic radiation forces between two adjacent bubbles are termed *secondary or mutual Bjerknes forces*.

Let's consider two bubbles whose centers are located at x_1 and x_2 as shown in Figure 3. The bubbles can have a different radius at rest, and the distance between their centers is $L = |\mathbf{x}_1 - \mathbf{x}_2|$. The bubbles are subjected to an acoustic field, and as a response, they vibrate and experience primary Bjerknes forces. In this section, only their interaction force is considered. The secondary acoustic radiation force acts along the vector connecting the centers of the bubbles.

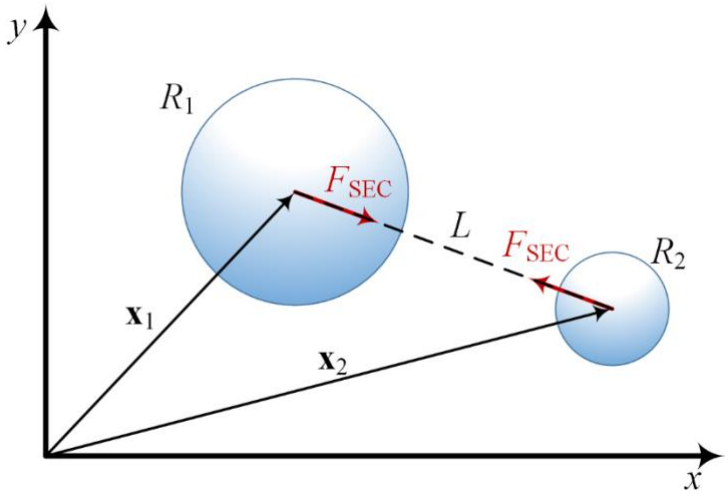

Figure 3. The geometry of a bubble pair.

Assuming that the bubbles are widely spaced yet their distance is much smaller than the acoustic wavelength (i.e., $\lambda >> L >> R_{10}+R_{20}$), where R_{10} and R_{20} are the first and second bubbles' radii at rest, we consider the response of each bubble to the incident wave field to estimate their vibrations

according to Eq.(25). The pressure field scattered by each bubble can be computed, and the force acting between the bubbles can be computed using Eq.(23) as:

$$F_{\mathrm{SEC}} = -\left\langle V_{b1}\nabla p_{b2}\right\rangle = -\left\langle V_{b2}\nabla p_{b1}\right\rangle. \tag{30}$$

where V_{b1} and V_{b2} are the instantaneous volumes of the first and second bubbles, and P_{b1} and P_{b2} are the scattered pressure fields from the bubbles. The convention is that positive force is attractive while negative force is repulsive. Plugging in the terms for the instantaneous volume and pressure, we obtain[9]

$$F_{\mathrm{SEC}} = \frac{2\pi R_{10}R_{20}A^2\left[\left(1-\omega_1^2/\omega^2\right)\left(1-\omega_2^2/\omega^2\right)+\delta_1\delta_2\right]}{\rho_0\omega^2L^2\left[\left(1-\omega_1^2/\omega^2\right)^2+\delta_1^2\right]\left[\left(1-\omega_2^2/\omega^2\right)^2+\delta_1^2\right]}, \tag{31}$$

where ω_1, ω_2, δ_1, and δ_2 are the natural frequencies and total damping terms of each bubble. From Eq.(31) it can be seen that if the bubbles oscillate in phase (i.e., $\omega_1,\omega_2<\omega$ or $\omega_1,\omega_2>\omega$) they attract each other, and when they oscillate out of phase (i.e., $\omega_1>\omega>\omega_2$ or $\omega_1<\omega<\omega_2$) they repel each other. This result fails to explain the bubbles' behavior in close proximity. To address this, the mutual interaction between the bubbles can no longer be ignored as shown by Zabolotskaya[14]. In this case, the coupled equations describing their vibration are:

$$\begin{aligned}
\ddot{R}_{\varepsilon1}+\omega\delta_1\dot{R}_{\varepsilon1}+\omega_1^2R_{\varepsilon1}+\frac{R_{20}^2\ddot{R}_{\varepsilon2}}{R_{10}L} &= -\frac{p_1(\mathbf{x}_1,t)}{\rho_0R_{10}},\\
\ddot{R}_{\varepsilon2}+\omega\delta_2\dot{R}_{\varepsilon2}+\omega_2^2R_{\varepsilon2}+\frac{R_{10}^2\ddot{R}_{\varepsilon1}}{R_{20}L} &= -\frac{p_1(\mathbf{x}_2,t)}{\rho_0R_{20}}.
\end{aligned} \tag{32}$$

This results in an updated equation for the bubble-bubble interaction force:

$$\begin{aligned}
F_{\mathrm{SEC}} &= \frac{2\pi R_{10}R_{20}A^2}{\rho_0\omega^2L^2\Delta}\left[\left(\frac{\omega_1^2}{\omega^2}-1+\frac{R_{10}}{L}\right)\left(\frac{\omega_2^2}{\omega^2}-1+\frac{R_{20}}{L}\right)+\delta_1\delta_2\right],\\
\Delta &= \left(\delta_2\left(1-\frac{\omega_1^2}{\omega^2}\right)+\delta_1\left(1-\frac{\omega_2^2}{\omega^2}\right)\right)^2+\left(\frac{R_{10}R_{20}}{L^2}-\left(1-\frac{\omega_1^2}{\omega^2}\right)\left(1-\frac{\omega_2^2}{\omega^2}\right)+\delta_1\delta_2\right)^2.
\end{aligned} \tag{33}$$

Immediate interpretation of the bubbles' behavior is not clear, but it can be shown that the direction of the force depends on their distance, L, which is not the case for the basic model (i.e., Eq.(31)). For example, when the natural frequencies of both bubbles are lower than the excitation frequency, but one is close to it, this can lead to a change in the direction of the force, generating stable and unstable equilibrium distances as shown in Figure 4.

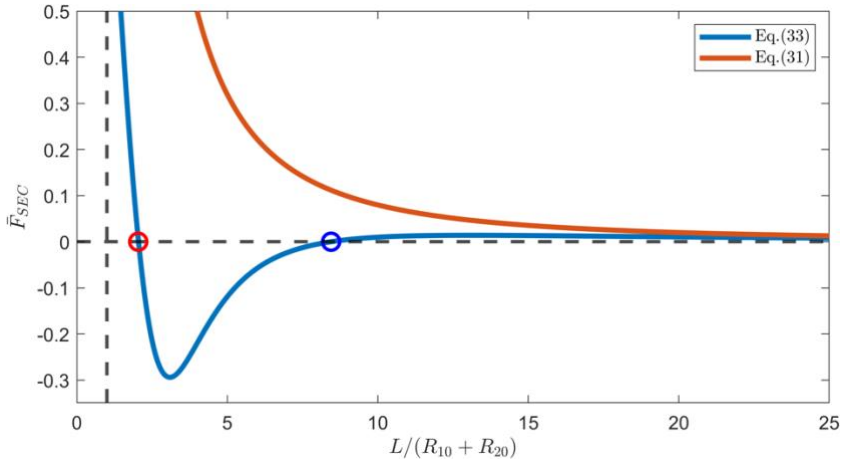

Figure 4. The normalized secondary Bjerknes forces as a function of the normalized distance according to two models, for bubbles with a natural frequency lower than the acoustic field frequency – ω_1, $\omega_2 < \omega$.

We can approximate the bubbles' natural frequency as[11]

$$\omega_0 = \sqrt{\frac{3\gamma p_0}{\rho_0 R_0^2} - \frac{2\sigma}{\rho_0 R_0^3}} \tag{34}$$

where γ is the ratio of specific heats for gas and σ is the surface tension. Figure 4 depicts the computed forces according to the simplified model which is suitable for $\lambda >> L >> R_{10}+R_{20}$ (i.e., Eq.(31)) and the latter model (i.e., Eq.(33)) that considers mutual interaction between the bubbles and is suitable for $\lambda >> L \sim R_{10}+R_{20}$. The values of the parameters that were used to compute the plotted forces are:

$$\begin{gathered}\rho_0 = 1000\,\mathrm{kg/m^3}, \quad \sigma = 0.072\,\mathrm{N/m}, \quad \gamma = 1.4, \quad p_0 = 101.325\,\mathrm{kPa}, \quad f = 130\,\mathrm{kHz}, \\ R_{10} = 25.4\,\mu\mathrm{m}, \quad f_1 = 128.39\,\mathrm{kHz}, \quad \delta_1 = 0.10, \\ R_{20} = 30\,\mu\mathrm{m}, \quad f_2 = 108.82\,\mathrm{kHz}, \quad \delta_2 = 0.06.\end{gathered} \tag{35}$$

c. Drag and thrust-induced acoustic streaming

The pressure and velocity fields vary with time in homogenous quiescent acoustic fields. When the time-averaged velocity does not nullify, mean fluid motion exists, which is termed *acoustic streaming*[3]. Acoustic streaming can be classified according to its driving mechanisms[15]. The energy of high-amplitude acoustic beams in open spaces is dissipated within the fluid over some distance, and pseudo momentum is transferred to the fluid and sets it in motion. This type of streaming was described by Eckart[16], and is not the focus of this chapter. Herein, the focus is on

the acoustic streaming occurring at the microscopic scale near boundaries at ultrasound frequencies. The boundary layer driven streaming is the result of the shear viscosity close to the boundary. The acoustic streaming regime is described in two domains, inside the boundary layer ($<\delta = (\nu/\omega)^{1/2}$) and is termed inner streaming, and outside the boundary layer ($>\delta$), and is termed outer streaming. Other classes of streaming are discussed in detail by Boluriaan and Morris[15].

To compute the acoustic streaming, one needs the governing equations for the fluid, namely the mass and momentum conservation laws without neglecting the viscosity, which is[3,10]

$$\rho\frac{\partial \mathbf{v}}{\partial t}+\rho(\mathbf{v}\cdot\nabla)\mathbf{v}=-\nabla p+\mu\nabla^2\mathbf{v}+\left(\mu_b+\frac{1}{3}\mu\right)\nabla(\nabla\cdot\mathbf{v}). \tag{36}$$

where μ is the shear viscosity and μ_B is the bulk dynamic viscosity. The medium is assumed to be homogenous and quiescent, and the acoustic field parameters are approximated similarly to Eq.(5) , while considering additional terms that do not oscillate at the same frequency as the first-order terms.

$$p=p_0+p_1+p_2+...,\quad \rho=\rho_0+\rho_1+\rho_2+...,\quad \mathbf{v}=\mathbf{v}_1+\mathbf{v}_2+... \tag{37}$$

Substituting Eq.(37) to Eq.(1) and Eq.(36), collecting terms of the same order and computing the time average[3,17,18], to the zeroth order one obtains (notice that $\langle\partial\bullet/\partial t\rangle=0$, and $\langle\bullet_1\rangle=0$):

$$\nabla p_0=0. \tag{38}$$

This means that the pressure is uniform, as expected. To the first order, one obtains no equation, as the time derivatives and the time average of the first-order terms equals zero. In the second order, the equations become:

$$\rho_0\nabla\cdot\langle\mathbf{v}_2\rangle=-\nabla\cdot\langle\rho_1\mathbf{v}_1\rangle,\quad \mu\nabla^2\langle\mathbf{v}_2\rangle+\left(\mu_b+\frac{1}{3}\mu\right)\nabla\nabla\cdot\langle\mathbf{v}_2\rangle-\langle\nabla p_2\rangle=\left\langle\rho_1\frac{\partial\mathbf{v}_1}{\partial t}\right\rangle+\rho_0\langle\mathbf{v}_1\cdot\nabla\mathbf{v}_1\rangle. \tag{39}$$

These equations can be solved analytically but only for select cases. For the rest of the cases, they can be solved numerically[15], using finite elements analysis[18,19] or direct numerical simulation[20].

The two methods that are experimentally used to generate acoustic streaming at the microscale are sharp-edge streaming[21–24] and bubble-induced streaming[25–28]. For both cases, the driving mechanism is viscous energy dissipation in the boundary layer, and for both, obtaining an

analytical solution is possible in a variety of cases. For sharp edge streaming, the interested reader is referred to Ref.[23], and for a trapped bubble, to Ref.[25,26,29].

3. Acoustic micromanipulation techniques

There are three types of forces that are relevant for micromanipulation: Primary acoustic radiation force (F_{PRI}), secondary acoustic radiation force (F_{SEC}), and drag or thrust induced acoustic streaming (F_{ST}). The description of these forces is discussed in Section 2. Primary acoustic radiation forces are applied to objects in intense acoustic fields. When the particle size is considerably smaller than the acoustic wavelength ($R<<\lambda$), this force can be computed using Gor'kov potential (Eq.(22)). The sign of the force is determined by the density and compressibility of the particle and fluid, and it may be attracted to either the nodes or antinodes (Figure 5A). For air bubbles, the sign of the primary acoustic radiation force, which is exclusively referred to as the primary Bjerknes force, may change as well, but due to a different mechanism (Eq.(29)). Bubbles are deformable and can resonate, and according to the ratio of their natural frequency to the acoustic field frequency, they can be attracted to either the nodes or antinodes. The natural frequencies of the bubble highly depend on its radius at rest, Eq.(34).

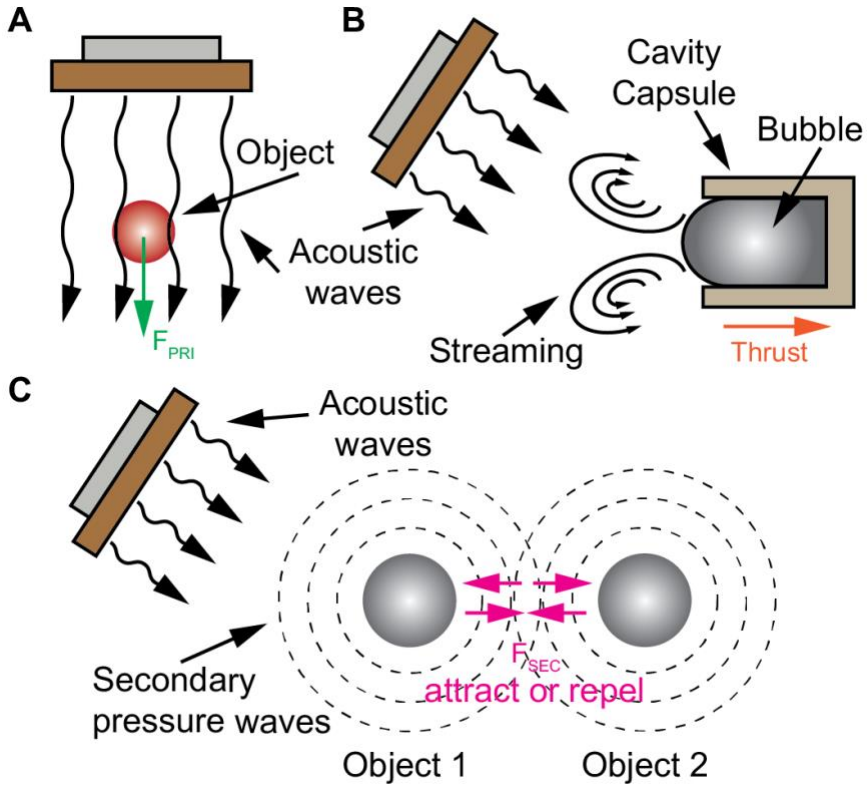

*Figure 5.Acoustic forces acting on objects submerged in fluid **A**. Primary acoustic radiation force, **B**. Acoustic streaming force, and **C**. Secondary acoustic radiation force*

Secondary acoustic radiation forces are generated by secondary sources, such as oscillations of bubbles excited by the primary acoustic field (Figure 5C). When the excitation frequency is close to one of the bubble natural frequencies, it vibrates with large amplitudes and generates a secondary acoustic field. Through these secondary fields, objects apply secondary acoustic radiation forces on each other. The sign of the secondary acoustic radiation force depends on the natural frequencies of the bubbles as well as the primary excitation frequency. (see Figure 5C, Eq.(31) and Eq.(33)). Additional nonlinear acoustic effect is acoustic streaming (see Eq.(39) in Section 2.2c), which can be generated around oscillating objects (Figure 5B). During the oscillation, there is a momentum exchange between the vibrating object and the surrounding medium in the viscous boundary layer. The acoustic streaming flow near vibrating objects is commonly observed as counter-rotating vortices. We further discuss acoustic streaming to actuate micro/nanorobotic devices in Section 4.

3.1 Introduction to Acoustic Tweezers

In this section, we describe acoustic micromanipulation techniques that are based on one or a combination of the aforementioned acoustic phenomena. We focus on the manipulation schemes that utilize bulk acoustic waves (BAW) because they are more suitable for medical applications.

Acoustic tweezers are based on the concept that an acoustic trap (or traps) can be created at a precise and controlled location in space. The trap is usually formed at a focal or a nodal point by acoustic radiation forces. Acoustic tweezing devices utilize longitudinal waves in fluids and a combination of longitudinal and transverse waves for on chip devices to manipulate objects in a controllable fashion.

Since the invention of the “acoustic tweezing” concept[30], numerous experimental platforms have been introduced for the non-invasive manipulation of biological samples[31]. Acoustic tweezers can be divided according to the type of waves they employ: surface acoustic wave (SAW) and bulk acoustic wave (Figure 6). SAW tweezers are particularly suited for on-chip manipulation of particles and biological samples[32]. Longitudinal, transverse, and Rayleigh surface waves[33] are generated and propagated along the surface of an elastic solid medium (Figure 6A). The energy of the waves leaks into the fluid medium residing on the surface, and pressure nodes and antinodes

are generated. Since the amplitudes of SAWs decay exponentially in the elastic media, the pressure in the coupled media diminishes spatially, allowing manipulation of objects only in proximity to the surface.

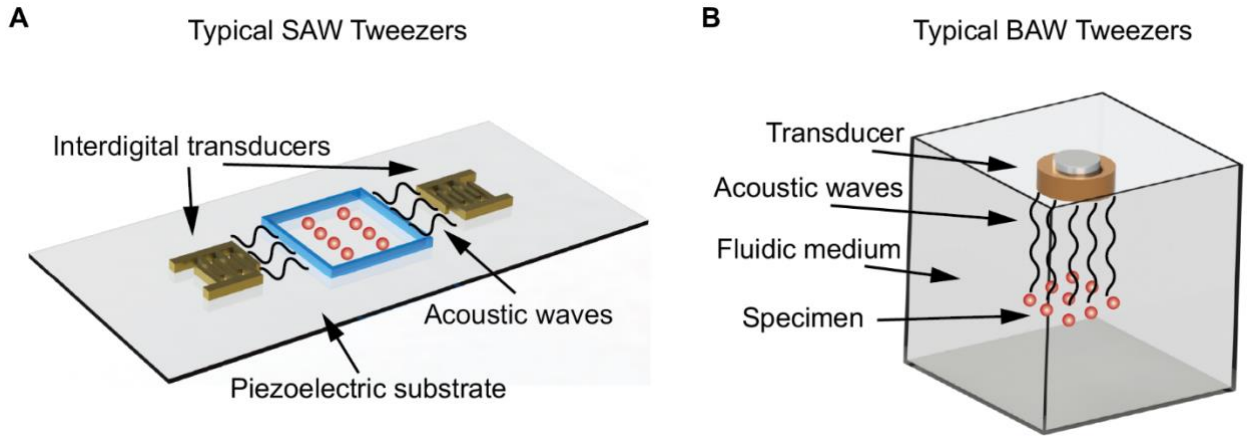

*Figure 6. Schematics showing typical **A**. SAW and **B**. BAW tweezers.*

BAW tweezers employ longitudinal pressure waves that propagate through the medium (Figure 6B). The acoustic pressure field is controlled through the transducers' spatial position and their relative amplitude, phase, and frequency. Additionally, BAWs can be focused to apply high pressure on select objects within spatially-resolved regions in the 3D workspace. In addition to serving as the primary acoustic source for direct micromanipulation, BAWs can excite structures with entrapped air bubbles[34] or sharp-edged solid features[35] to generate secondary forces. These acoustically-excited mechanical microsystems can be used to manipulate particles, cells, and multicellular organisms. The working principles of this actuation scheme and how microrobots can be powered with acoustic waves are described in detail in Section 4. In the remaining of Section 3, we focus on BAW tweezers and associated micromanipulation techniques because these are better suited for medical applications.

3.2 Acoustic micromanipulation using bulk acoustic waves

There are two major approaches to realize BAW tweezers (Figure 7). In the first approach a standing wave field is generated in the medium. Early examples of particle tweezing using standing

waves in air date back to the 1930s.[36] It was later quantitatively shown that acoustic waves can manipulate air bubbles in water.[37,38] Rigorous theoretical analysis followed those seminal experimental demonstrations.[5–7,9,13,14,38] Due to the ease of use and interesting physics, air bubbles and oil droplets have been used extensively to explore the mechanics of BAW tweezers. Bubbles and droplets are size controllable and compressible; therefore, all the acoustic forces can be studied and utilized. Bjerknes was one of the first scholars who discussed the behavior of an air bubble in an oscillating media,[39] and bubble dynamics was studied by exciting them in a standing wave fields.[38,40]

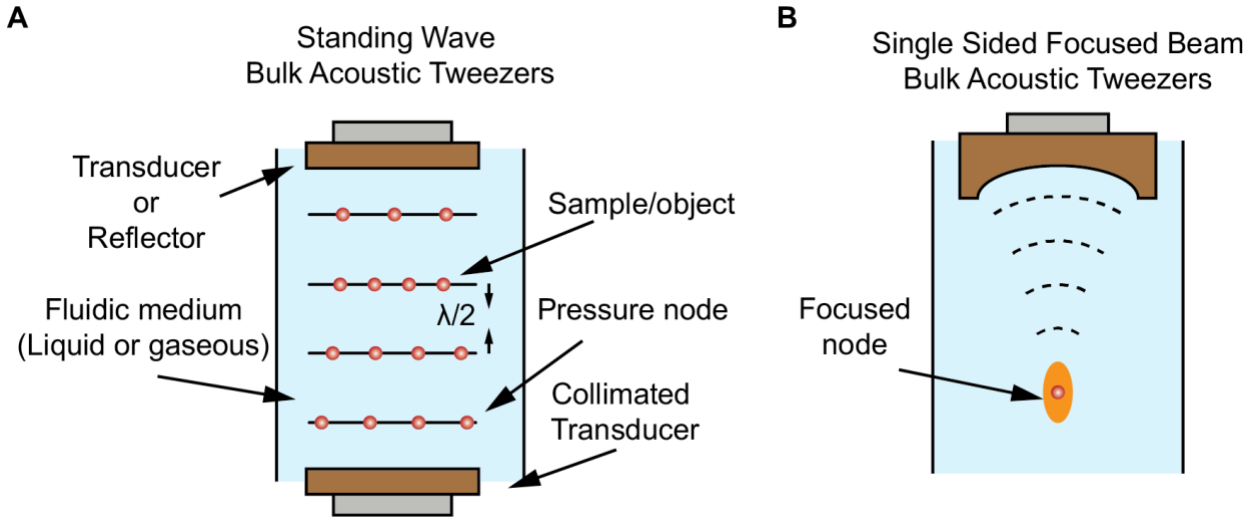

Figure 7.Illustration of conventional bulk acoustic tweezers. ***A****. Typical BAW-based standing acoustic wave tweezer. Either two transducers or a transducer and a reflector can be employed to form traps- pressure nodes and antinodes.* ***B****. A representative configuration.*

One of the most widely used techniques to generate a standing wave field is to use two identical transducers facing each other so that they would generate identical waves propagating in opposite directions (Figure 7A). Alternatively, a transducer and a reflector can be placed in a way that the generated and reflected sound waves would interfere to form a standing wave with the desired distribution of nodes and antinodes.[41]. In a perfectly collimated system, the pressure nodes are spaced half of a wavelength apart. The same is true for the antinodes. Objects in the field move to the closest acoustic trap (i.e., either pressure node or antinode), where the displacement is always less than half of a wavelength.

Due to acoustical phenomena that mitigate the wave energy as it propagates in the media (e.g., dispersion and attenuation), the transducers and reflectors are often placed closely, usually several half wavelengths apart. For efficient tweezing, the size of the object must be much smaller than the wavelength wave (i.e., $R << \lambda$). If the size of the object is larger, the theoretical equations no longer hold, and the resulting forces diminish. The signal fed to the transducers usually comprises a single harmonic whose amplitude, frequency and phase are controlled using a signal generator. In most applications, an amplifier is required to drive the acoustic transducers, which are usually made of piezoelectric materials. The deformation of the piezoelectric material with the application of voltage produces the pressure field. The excitation frequencies are set by considering the topology of the generated pressure field, also, they should correspond to the resonance frequencies of the transduces for efficiency.

Acoustic tweezing in air is called acoustic levitation, as the acoustic forces counteract gravity making the trapped particles levitate. The dominant forces in acoustic levitation are the primary acoustic radiation and drag forces. The drag force (F_D) is generated by acoustic streaming. F_{PRI} acts to trap the object in the node or antinode while F_D makes the tweezing unstable. The F_{PRI} is proportional to the volume of the sample, while F_D is proportional to the radius of the object according to the Stoke's law assuming that Re < 1. When Re > 1, the Schiller-Naumann model can be used to obtain more accurate values.[42] Therefore, F_D / F_{PRI} increases as we scale down the size of the objects. Stability problems occur when the F_D / F_{PRI} is between 0.25 and 0.75.[43,44] For values higher than 0.75, the acoustic levitation and trapping become unstable.

Tweezing based on focused ultrasound has been proposed to address the instability problem while considering safety issues. The higher acoustic pressure, P, results in a higher acoustic radiation force ($F_{PRI} \sim P^2$). The focused ultrasound transducers usually employ sound waves of higher frequencies compared to standing wave platforms. The higher frequency results in a shorter wavelength (Eq.(13)), which leads to a higher spatial resolution. This is particularly useful to trap and maneuver small objects (from tens of micrometers to nanometers). The standing wave focused ultrasound systems typically have two transducer bowls facing each other.[30] They are positioned to focus the acoustic beam at the center in a confocal arrangement.

Wu[30] introduced the term “acoustical tweezers”, a dual beam method using two opposing acoustic waves in the Rayleigh regime where the particle much smaller than the wavelength, $R<<\lambda$. Latex spheres (diameter of 270 μm) and frog eggs were successfully trapped by employing sound waves at 3.5 MHz ($\lambda\approx0.43$ mm).

The force applied on an object can be calculated using the gravitational escape method. Particles are placed in the center of the acoustic beam. Then, the pressure level is varied from high to low until the particles escape. The pressure levels are recorded for several different particles. Then, the resultant force can be calculated.[45] Comparison of the sizes, frequency and forces in the acoustical tweezers and microrobots are further discussed in the Section 4.

Standing wave bulk acoustic tweezers and standing wave focused ultrasound tweezers require the objects to be surrounded by the transducers, which limits the translation to the clinics. Moreover, standing wave fields consist multiple equilibrium positions in the workspace that apply forces and trap untargeted objects. The multiplicity of nodes and antinodes leads to the existence of multiple trapping sites that cannot be moved independently. It is ideal to generate forces only on the target object. To resolve these issues, techniques were developed to manipulate particles using transducers from a single side (Figure 7B).[46] These techniques are based on acoustic lenses, transducer arrays and vortex beams (Figure 8).

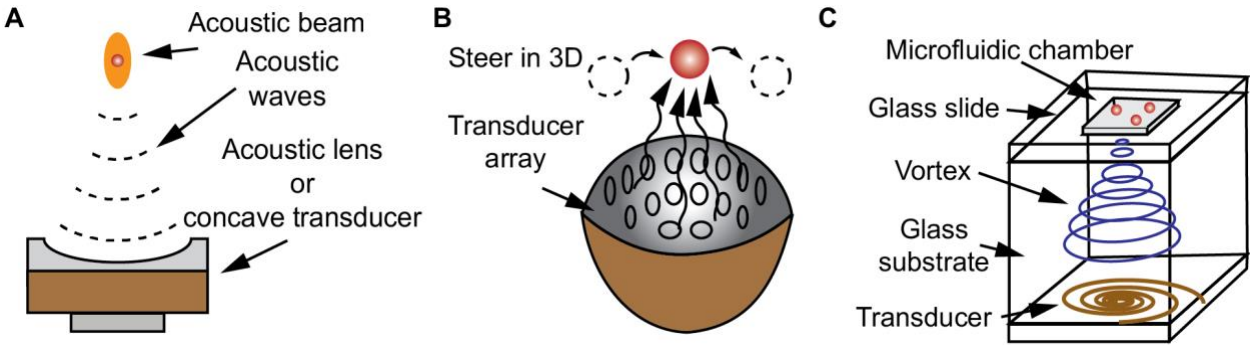

Figure 8. Single-sided acoustic tweezers. ***A****. The acoustic beam is tightly focused using either a transducer with an adjacent acoustic lens or a concave transducer.* ***B****. An array of acoustic transducers is used to 3D-steer a bead in a gaseous media by changing the phase between transducers.* ***C****. An acoustical vortex tweezer is used to trap beads in microchannels. The acoustic waves are transmitted via a glass substrate from the transducer to the microchannel. The 2D steering is achieved by moving the microchannel using an automated stage.*

The radiation force on the particle is exerted through momentum transfer, which is due to reflected and refracted acoustic rays. Refraction is the primary phenomenon causing the particle to move towards the beam's center. Therefore, the acoustic impedance of the particles and surrounding media needs to be matched.[47] The force in the tight focus depends on particle size, and excitation frequency. To generate a tight focus, either the transducers have a curved geometry or an acoustic lens is used with a flat transducer (Figure 8A).[48,49]. One of the important parameters is f-number, $f_{number} = \frac{\text{focal distance}}{\text{lens diameter}}$, which is the ratio of focal distance to the lens diameter. The f_{number} is usually chosen less than 1 to keep the focal point tight and limit the energy loss due to attenuation. In addition, to increase the spatial resolution higher frequencies are used. For example, in 126-µm-diameter oleic acid droplets, transducers with a resonance frequency of 30 MHz can be employed.[47]

Single beam levitation by focusing the acoustic rays using either single-sided curved transducers or transducers with acoustic lenses is promising for several applications such as particle manipulation and drug delivery *in vivo*. However, their maneuverability (translation and rotation of the traps) is limited. Furthermore, the energy loss, especially when using an acoustic lens can be high which lessens the applicability in biologically sensitive media.[50]

To address these problems, an array of acoustic transducers can generate multiple acoustic traps and maneuver particles simultaneously. (Figure 8B) This method employs acoustic radiation forces[51] and acoustic streaming[52] to levitate objects. The location of the traps are controlled by changing the relative phase and amplitude of the transducers. Thus, no physical transducer movement is required to maneuver objects. Different structure arrays such as plane and vertical have been implemented in liquids and air.[53,54] It was shown, that particles (usually smaller than 1 mm) can be translated and rotated along a 3D path without moving the arrays using a so-called acoustic holograms.[51,55]

These acoustic holograms demonstrate two important features. The first is that single-sided arrays can trap microparticles and levitate them by generating forces at the order of µN, thus counteracting gravity. The second is that, the topology of the acoustic field can be tuned on the fly. These allows controlling multiple particles in acoustic fields, thus paving the way for biomedical applications, e.g., microsurgery without physical interference.

Acoustic holograms are promising for several *in vivo* and *in vitro* tweezing applications; however, they are challenging to scale down to single cell size. SAW tweezers generate acoustic waves on the surface of piezoelectric substrate (usually $LiNbO_3$), resulting in either grids or lines of nodes and antinodes. This leads to multiplication of trapping areas. Therefore, it is challenging to trap and manipulate single objects (e.g., cells). This challenge can be addressed using acoustical vortex tweezers which can tightly focus the helical acoustical waves and generate a single trap to maneuver objects on the scale of hundreds of micrometers to tens of micrometers (cell size). The schematic in Figure 8C illustrates a typical acoustical vortex tweezers.[56] The device is comprised of a piezoelectric substrate at the bottom, a microchip at the top filled with a liquid medium and samples, and a glass substrate bridging the bottom and top subparts. The piezoelectric substrate has a unique crystallography that allows out-of-plane pressure distribution upon electrical signal. The design of spiraling active electrodes forms a vortex and focalizes it inside the microfluidic chip. The electrodes are made of thin layers of metals (usually Ti/Au and Cr/Au). A sinusoidal electrical signal is applied to generate localized deformation around the interdigitated transducers. A bulk acoustical vortex normal to piezoelectric substrate is generated and transmitted to the microchip through the glass in the middle. The working mechanism of the acoustical vortex

tweezers is based on Bessel beams and Hankel beams.[57–59] The contribution of Bessel beams converges to none with the distance. Therefore, Hankel contribution is the main reason of focal area formation.

The size limit of the maneuverable particles is dictated by the focal area of the vortex in the microchip. The size of the focal area can be controlled by design. For instance, a 4.4 MHz[57] and 47 MHz[56] spiraling transducers can trap 75 µm and 7 µm particles, respectively. The pressure and, in turn, the resulting force, is adjusted by the applied signal. The operation frequency and signal amplitude along with material properties are the key parameters to determine the forces. Up to 200 pN were applied to trap single cells and manipulate them in a designated route.[56] One of the main challenges in acoustofluidic applications is joule heating in relatively long experiments. In the acoustical vortex tweezer set-ups, due to the distance between focal points and piezoelectric substrates, joule heating at the microchip is minimal even during long experiments (tens of minutes).

Even though vortex tweezers are currently designed for on chip applications, they have the potential to be translated to clinics. Current acoustical vortex tweezers are designed to be operated close to the acoustical source. With an ergonomic design of the middle structure (currently glass), the acoustic waves can be transmitted to human organs for a selective manipulation of samples.

4. Micro/nanorobotic devices actuated by acoustic fields

As discussed in the previous sections, acoustically excited structures can generate steady flows and secondary acoustic radiation forces. In this section, we discuss how robotic devices can be designed, powered, and controlled through these acoustic phenomena. Although proof-of-principle examples have been realized using a variety of transducers and acoustic fields, we anticipate that bulk acoustic waves will be used in clinical applications. The section starts with relatively simple mobile micromachines and continues with more complex robotic devices that can perform dexterous micromanipulations.

4.1 Mobile acoustic micromachines

The overall propulsion scheme is based on an actuator that convert acoustic energy into thrust. A gaseous bubble or microfabricated structure (e.g., beams and membranes) can act as such by converting the acoustic waves into mean flow (i.e., acoustic streaming) thus generating thrust for propulsion.

We first describe how a gas bubble entrapped inside a microfabricated cavity can be used as an on-board thruster. Upon acoustic excitation, due to the compressibility of the bubble, the bubble oscillates at the liquid-air interface prescribed by the opening of the cavity. These oscillations are maximized when the sound field frequency coincides with the resonance frequency of the bubble. Then, the bubble's oscillations resemble the corresponding mode shape.[27,60] As discussed earlier, acoustically-excited bubbles experience three different forces: primary acoustic radiation force (F_{PRI}), secondary acoustic radiation force (F_{SEC}), and acoustic streaming force, (F_{ST}). F_{SEC} is due to the interactions among nearby bubbles or the interactions of bubbles with solid boundaries. The thrust stems from the asymmetric design of the capsule, which results in a propulsive force (Figure 5B).[26,28] F_{PRI} is generally considered to be negligible in the actuation of bubble-based machinery.[61]

If the cavity or cavities are engraved on a suspended microstructure, oscillations of the bubble can lead to motion (Figure 9A). Using photolithography, sub-mm sized cylindrical capsules with a single opening were fabricated.[62] The micromachines moved as fast as 45 mm s^{-1} (50 body lengths per second). By tuning the design (i.e., shape of the structure, number of bubbles, and their distribution) swimmers capable of turning were realized. Bubble-based micromachines can be selectively actuated if they comprise distinct bubbles (i.e., different volume and opening).[63] The natural frequency of the bubble depends on its volume and opening size, therefore different micromachines can be activated at different frequencies.[27,60] Considering the typical size of the bubbles used in these studies,[28,63–65] and the motivation to excite the bubbles at their first natural frequency, the micromachines have been actuated at frequencies ranging from a few hundred kHz to several MHz. These studies have also shown that the micromachines generate high enough forces allowing them to move inside highly viscous and viscoelastic media. This feature is important for *in vivo* application considering the rheology of bodily fluids such as blood and

mucus. The materials that were used to microfabricate these structures, Parylene and PEG, are biocompatible and are widely used for *in vivo* biomedical applications.

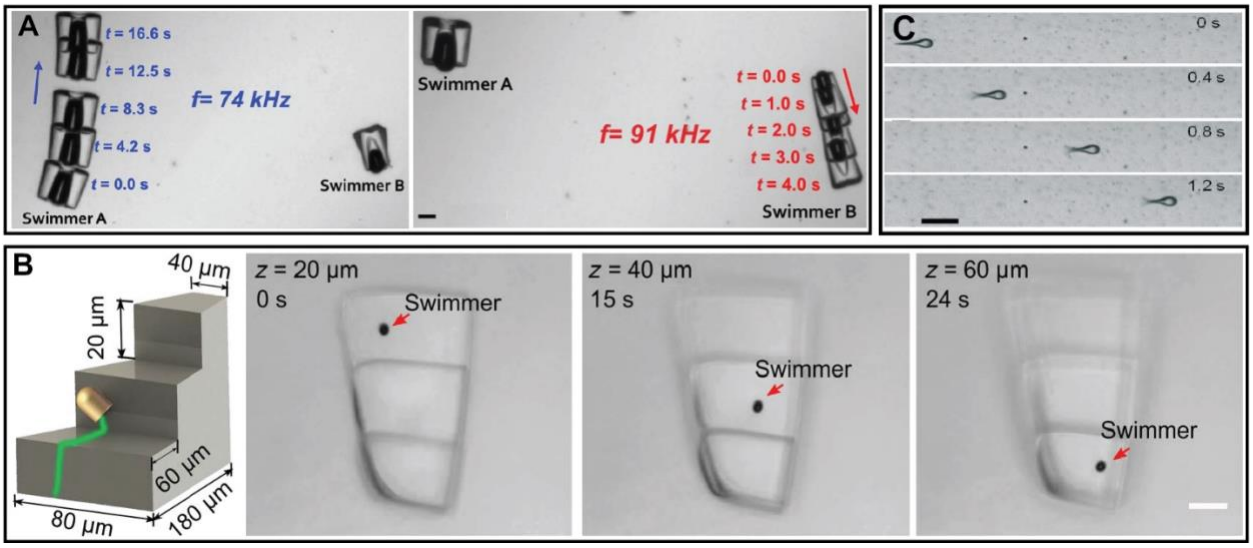

Figure 9. Mobile acoustic micromachines based on bubble and sharp-edge. ***A****. Swimmers of different microbubbles sizes were excited using various excitation frequencies. Selective actuation enabled to control the swimmer's motion.* ***B****. A nanoprinted free swimmer with microbubble was actuated via acoustic filed while the direction of the swimmer was controlled using a magnetic field, which allowed the swimmer to follow a 3D trajectory.* ***C****. A monolithically fabricated microswimmer with sharp-edges was excited by acoustic waves. Upon actuation, the tail oscillated at higher amplitude than the head, which resulted in translational motion.*

The early prototypes had relatively large air bubbles entrapped in cavities due to the limited resolution of early photolithographic techniques. Recent work has shown that smaller acoustic micromachines can be fabricated with precise dimensions using the two-photon polymerization method.[28,64,66] Smaller bubbles have higher resonance frequencies, therefore 3D nanoprinted micromachines are excited at higher frequencies. For medical applications, this shift in actuation frequencies is desirable as the smaller micromachines can reach hard-to-reach regions in the body and be controlled by clinically-available ultrasound transducers.

In general, when air bubbles are close to rigid substrates secondary acoustic radiation forces emerge due to mirroring effect (i.e., a rigid boundary acts as a mirror, as if a similar bubble exists on its other side).[2] This force is always attractive, because identical bubbles always attract each

other. This attractive force acts in parallel to the thrust generated by the bubble induced acoustic streaming. As a result, bubble-based micromachines are attracted to walls of containers. (Figure 9B) These forces can be harnessed for motion control. For example, acoustic micromachines can move along a curved surfaces through a surface-slipping motion.[67] This mode of motion could be useful to navigate micromachines inside arteries and the gastrointestinal tract. This last study has recently been extended to locomotion inside viscoelastic fluids. A high shear rate propulsion mechanism was reported, which is a significant step towards applying these microrobots *in vivo*.[68]

Another common method to generate microstreaming employs sharp edge structures. These flexible structures oscillate under acoustic excitation and induces microstreaming at the tip.[17] Exciting the structures at moderate acoustic levels leads to a linear behavior; thus, each tip oscillates at the driving frequency with a proportional amplitude. These parameters, therefore, can be controlled via the input signal generated by an acoustic transducer. The concept of sharp edge streaming was explored to create microscale mixers[69] and pumps[70] within microfluidic channels. Later, rotary systems were developed by designing rotors fitted with extended arms with sharp-edged features.[71] The sharp-edges along with the compliance of the material leads to large oscillations at the tip at the designated driving frequency. The micromachines could rotate either clockwise or counterclockwise at distinct frequencies according to the design. It is reported that the angular speed is proportional to the number of sharp-edge streamers; each is attached to a single arm of a rotor. A 6-arm rotor span as fast as 1200 RPM. Later, this study has been extended to compound machinery by using the rotors inside microfluidic channels to drive microscale turbines and mills.[72]

Analogous to the bubble-based microsystems, the streaming flow can generate thrust that propels mobile micromachines forwards.[24] A micromachine, inspired by sperm cells, with a head and flagellum-like tail was developed (Figure 9C). The material properties and structural design maximized the oscillations at the tip of the tail. As a result, the micromachines move forwards as fast as 1200 μm s^{-1} (~8 body length per second). Similar machines were miniaturized further using electrodeposition. In this work,[73] although the thickness of the micromachine was fixed throughout the body (<1 μm), the oscillation amplitude due to structural resonance was maximized at the tail.

The oscillation at a frequency of approximately 90 kHz generated acoustic streaming and propelled the swimmer in aqueous media.

4.2 Soft Robotic Microsystems

The micromachines we discussed so far are displayed simple motions, i.e., translational, and rotational. Full 3D motion has also been realized by controlling multiple bubbles of different sizes on the same device[74]. Compliant mechanisms achieve force and motion control through elastic body deformation. One of the biggest advantages of using compliant mechanisms to create microscale robotic devices is that they can be fabricated as a monolithic structure through 3D printing. Moreover, unlike rigid mechanisms, compliant mechanisms do not suffer from surface forces as the transmission is based on deformation and not friction. Recent work has shown that capsules that entrap bubbles can be connected to flexible beams using two-photon polymerization.[28] The natural frequencies of the entrapped bubbles can be tuned by editing the cavity geometry, e.g., cavity opening diameter and number of openings, for selective actuation.[27,60] The flexible beams allow continuous motion under various acoustic forces (e.g., F_{ST}, and F_{SEC}). A single cavity with three openings that is linked to the surface with a flexible beam can follow prescribed trajectories due to F_{ST} (Figure 10A). Additionally, a linear actuator was developed by linking two cavities facing each other via a flexible spring.[28] The bubbles in the cavities generated F_{SEC} and thus attracted each other resulting in translational motion by deforming the beams. These actuators can serve as building blocks for soft robotic devices with more complex architectures and many degrees of freedom.

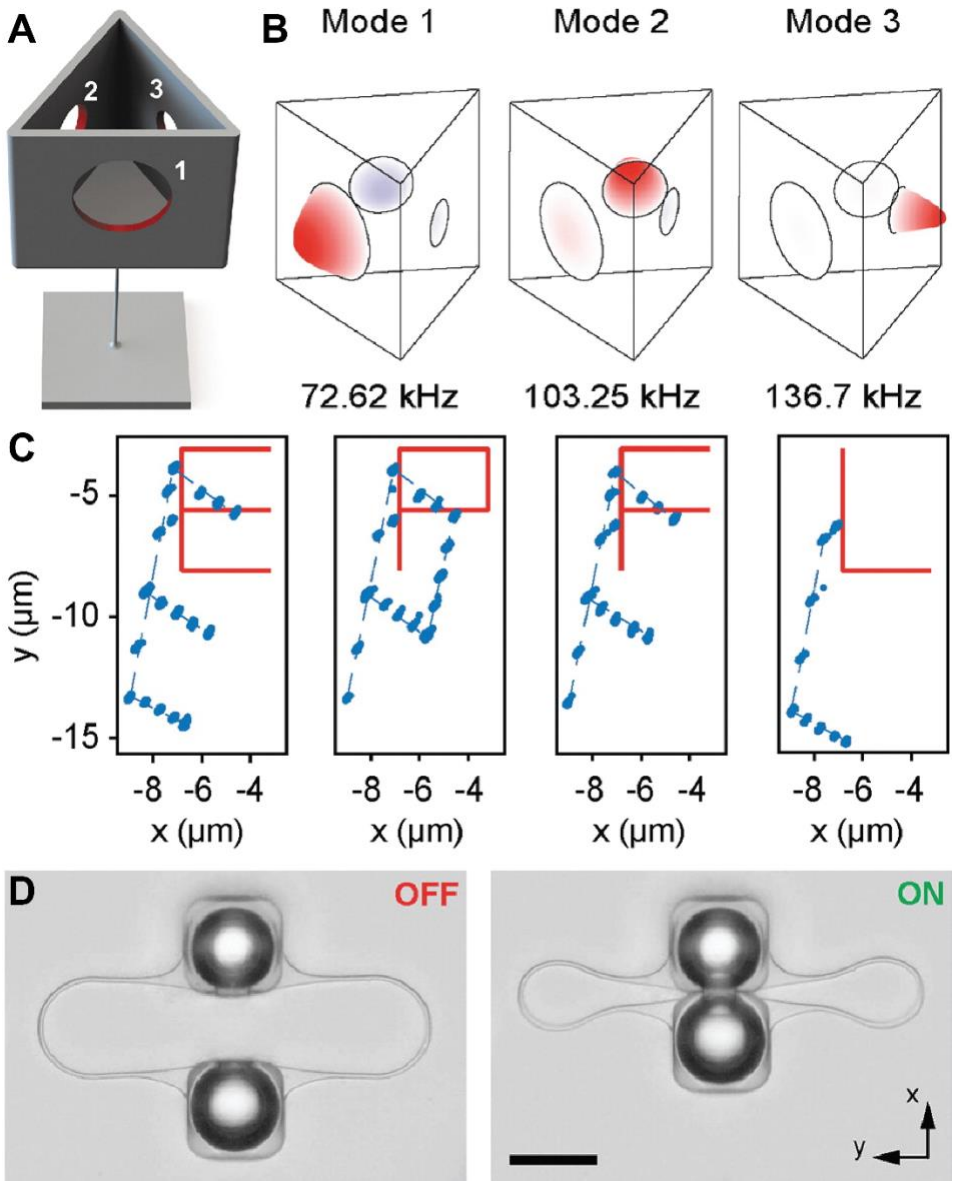

Figure 10. 3D nanoprinted soft robotic microsystems. ***A.*** *The illustration shows a capsule with three distinct orifices. The capsule is attached to a glass substrate via an elastic beam.* ***B.*** *The direction of the movement of the capsule was controlled via actuation of different modes of the entrapped air bubble.* ***C****. The markers show the tracked position of the capsule while it was moved along paths prescribing the letters "EPFL".* ***D****. Two capsules are connected with a spring, where the top one is fixed to the substrate and the other is free to move. Upon acoustic excitation, the capsules attract each other due to secondary acoustic radiation forces and the spring is compressed. Scale bar: 50 µm.*

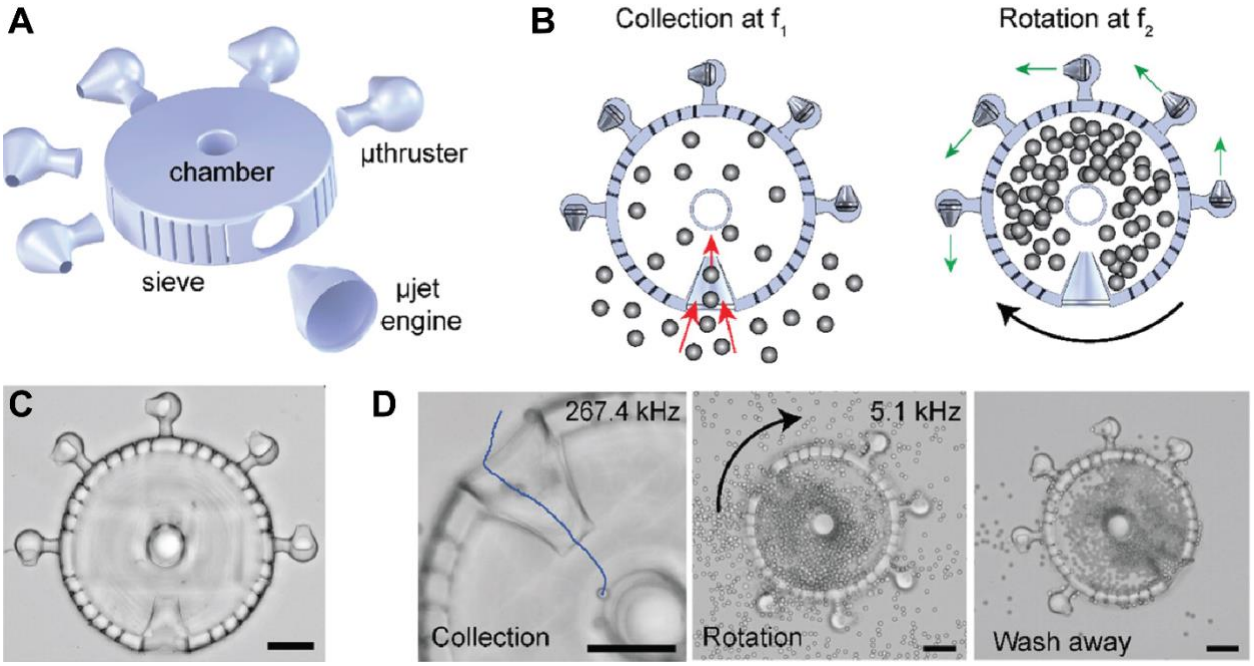

*Figure 11. An acoustically-powered soft robotic device. **A**. Schematic of the device highlighting the collection chamber, sieve for filtering, and a μjet engine for pumping media. **B**. Illustration showing sample collection and device rotation. **C**. A bright field image of the device. **D**. Time lapse images showing collection of particles, rotation of the device, and the final state after washing away the suspended particles. Scale bars: 75 μm.*

An alternative route to creating microrobotic devices is based on the use of sharp-edged hydrogel structures.[75] Monolithic rotary machines and pumps were fabricated inside microfluidic chambers from biocompatible polymers. The pumping of fluid was driven by microstreaming generated by 3D conical structures, where the flow velocity reached up to 476 μm s^{-1}. Taking advantage of 3D nanoprinting, a chamber and a sieve were added to the pump to collect samples from the media. As a step forward in the creation of complex functional devices, mass transport and selective actuation of thrusters were combined in a single device (Figure 10B). The resulting compound machine could rotate in place and collect microparticles from the surrounding medium in a spatiotemporally controlled fashion. Such untethered biomanipulation tools have the potential to be utilized *in vivo* as injectable drug delivery devices.

5. In vivo actuation of micro/nanorobotic devices

Acoustic manipulation technologies can serve as unique tools for fundamental research in life sciences and biomedical applications.[76,77] Here, we provide examples on how microscale devices can be manipulated inside a living animal. As described in the previous sections, there are various

ways of remotely translating and rotating objects using acoustic transducers, and bulk acoustic waves are best suited for in vivo applications. So far, the successful demonstrations contain basic trapping and translation of microscale objects. However, the platforms are capable of actuating micro/nanorobotic devices. It is only a matter of time before acoustically powered robotic devices are operated inside living animals.

The first example shows a steerable, vortex-based acoustic trapping beam to lift and move a 3-mm glass sphere inside the urinary bladder of a live pig.[78] A 256-element, focused array with a 12-cm focal distance was operated to generate the vortex beams with around 1.4 MPa pressure. The beam is created by altering the phase among the focused array of 256 transducer elements while their amplitude remains constant. The sphere is trapped at the center of the beam generated at 1.5 MHz, and moved in a plane transverse to the beam axis. No histological evidence of injury was observed in the pigs following ultrasound exposure, demonstrating the non-invasive nature of the technique.

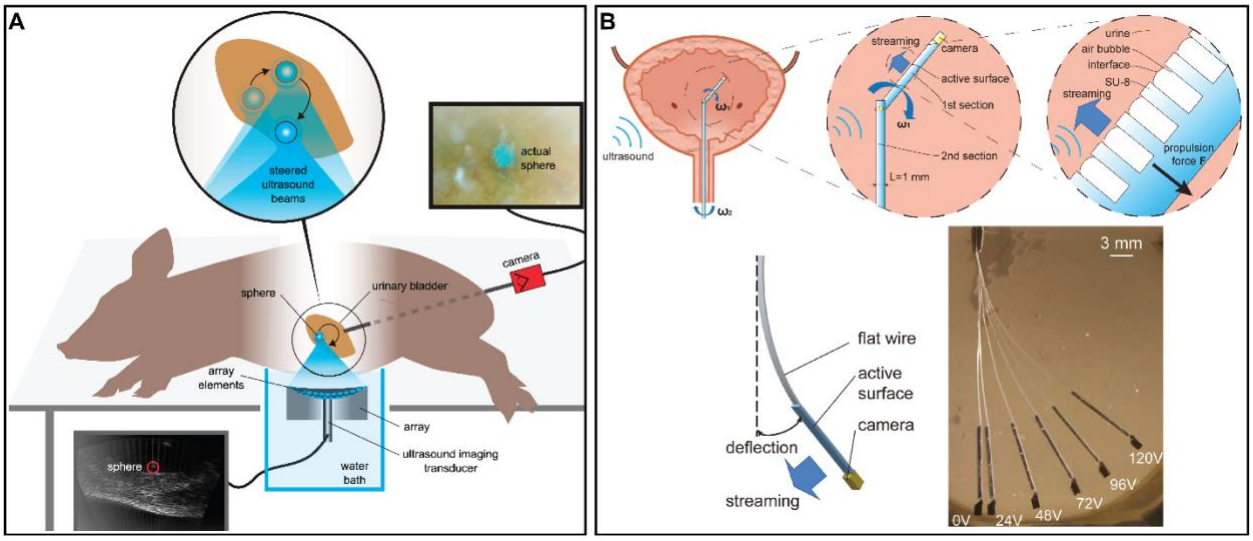

Figure 12. Demonstration of in vivo acoustic micromanipulation. ***A****. A 3-mm sphere is manipulated in a pig bladder using a bulk acoustic tweezer.* ***B****. (Top) Schematic of an acoustically powered miniaturized cystoscope. (Bottom) Illustration of a flexible arm bent due to acoustic streaming forces. The arm is deflected under acoustic field whose amplitude is controlled via input voltage.*

Scaling down the size of the objects would result in significantly lower primary radiation forces, which is a bottleneck for in vivo applications. On the other hand, as described in the previous sections, significantly higher forces can be generated on microbubbles. Microbubbles have been

increasingly used for biomedical applications such as targeted drug delivery. Notably, recent work has demonstrated ultrasound-mediated aggregation and uncaging of drug-loaded liposomes tethered to microbubbles inside the brain vasculature of rats.[79] Using this technique, small molecules are delivered with millimeter-precision, without opening the blood-brain barrier at relatively low pressure (around 100 to 300 kPa). The aggregation of microbubbles, which are 1.5 μm in diameter, is probably due to the secondary Bjerknes forces between the bubbles. After local aggregation at 2.5 MHz, the drugs are uncaged from the microbubbles with a second ultrasound pulse sequence with higher pressure. More recent work has shown that lipid-shelled microbubbles can be concentrated and manipulated for precise positioning within the blood vessels of mice using an acoustic vortex tweezer.[80] The acoustic waves are generated by four transducer elements that are driven by 3-MHz sine waves to produce pressures ranging from 80 to 800 kPa. The wave propagates along the z direction, and phase difference around the axis gradually varies from 0 to 2π radians in each x-y plane. The phase is indeterminate on the axis, which leads to the generation of a null core of zero amplitude, creating a vortex structure with a potential well. The particles near the well experience an inward force and thus can be trapped. In parallel, vortex beams were generated by eight independent transducers driven with the necessary time delays to construct a helicoidal wavefront.[81] The results showed that the trapping beam can operate in 3D after propagating through thick, opaque-to-light, viscoelastic media without suffering from wavefront distortion. It can be sharply focused to localized sites, offering a pinpoint control over an individual microbubble, even in crowded environments. Finally, a standing wave acoustic tweezer system has been developed where four piezoelectric actuators with a resonance frequency of 4.25 MHz were positioned orthogonally to each other around an off-centered fluidic channel.[82] This platform allows for two-dimensional manipulation of intravenously injected microbubbles inside zebrafish embryos.

As an alternative to primary and secondary radiation forces, acoustic streaming forces can be used to actuate medical devices. To our knowledge, there is only one medical device, a miniaturized urological endoscope, that is actuated following this strategy. Surfaces that consist of two-dimensional arrays of microbubbles were fabricated, which oscillate under ultrasound excitation and thereby generate an acoustic streaming force.[83] Mounting such a surface at the tip of a millimeter-scale endoscope realized remotely controlled bending and thus steering. Bubbles of

different sizes are addressed by their unique resonance frequency, thus multiple degrees-of-freedom can readily be incorporated. The flexible endoscope was tested in a rabbit bladder ex vivo.

6. Discussion and Outlook

Acoustic technologies are indispensable for medicine. Recent advances in acoustic micromanipulation have shown great potential to provide means for targeted drug delivery and alternative minimally invasive interventions. In this chapter, we summarized the physics behind the widely explored manipulation strategies and elaborated on the most exciting directions by going over proof-of-concept demonstrations. These demonstrations pave the way for the future development of more advanced medical applications and lay the groundwork for translating in vivo acoustic manipulation to human patients. In the coming years, we will surely see the development of more advanced in vivo acoustic manipulation technologies that will transport microscale robots to hard-to-reach tissues and deliver therapies with pinpoint accuracy, without posing either risks or side effects or post-operative trauma. We shall also expect to see remote acoustic steering of guidewires, catheters, and endoscopes for diagnostic and therapeutic operations in near future.

There are a number of factors that define the effectiveness and safety of these manipulation strategies. A broad range of frequencies (from kHz to MHz) have been utilized in acoustic tweezers and microrobotic applications[24,30,73]. In the majority of cases, the frequencies dictate the sizes of manipulable objects. As a reference, the speed of sound in water at room temperature is approximately 1500 m/s, and at 100 kHz the acoustic wavelength is 15 mm. Significant acoustic forces are generated when the size of the sample is much smaller than the wavelength $R << \lambda$. In addition, the distance from the acoustic source is important as the acoustic pressure attenuates with the distance due to dissipative losses.[1,12] As discussed, solid elastic particles with diameters of 190-390 μm can be trapped in aqueous media, where the resultant trapping force is on the order of 20 nN.[50] To scale down the size of the trapped particles, acoustic waves must be generated at higher frequencies, resulting in a smaller trapping area. Single cells (diameter of ~10 μm) were trapped using a 30 MHz focused transducer,[84] where the estimated force goes up to ~100 nN. The studies provide an order of magnitude estimate on forces that can be applied on microscopic objects through primary acoustic radiation forces. As a comparison, ultrasonic imaging uses frequencies

in the range of 2-18 MHz. Acoustic streaming and secondary acoustic radiation forces may provide ways to apply higher forces on microscale objects as they scale more favorably compared to the primary acoustic radiation force. The work summarized in this chapter provides general guidelines on how to harness these secondary forces to power microrobotic devices. The future is vibrant for acoustics resonating with microrobotics.

7. Acknowledgment

Murat Kaynak is supported by the Swiss National Science Foundation (SNSF) under the postdoc mobility fellowship (Project number: P500PT_211084). Amit Dolev acknowledges the support of the European Research Council under the European Union's Horizon 2020 Marie Sklodovska-Curie Actions Postdoctoral Fellowship (Grant agreement No. 101022448).

8. References

1. Pierce, A. D. *Acoustics: an introduction to its physical principles and applications*. (Springer International Publishing, 2109).
2. Leighton, T. *The Acoustic Bubble*. (Academic Press, 2012).
3. Hamilton, M. F. & Blackstock, D. T. *Nonlinear Acoustics*. (Academic Press, 1998).
4. Blackstock, D. T. *Fundamentals of physical acoustics*. (Wiley, 2000).
5. King, L. V. On the acoustic radiation pressure on spheres. *Proc. R. Soc. London. Ser. A - Math. Phys. Sci.* **147**, 212–240 (1934).
6. Yosioka, K; Kawasima, Y. Acoustic Radiation Pressure on a Compressible Sphere in a Viscous Fluid. *Acta Acust. united with Acust.* **5**, 167-173(7) (1955).
7. Gor'kov, L. P. On the forces acting on a small particle in an acoustical field in an ideal fluid. *Sov. Physics-Doklady* **6**, 773–775 (1962).
8. Karlsen, J. T. & Bruus, H. Forces acting on a small particle in an acoustical field in a thermoviscous fluid. *Phys. Rev. E - Stat. Nonlinear, Soft Matter Phys.* **92**, 043010 (2015).
9. Doinikov, A. A. Bjerknes forces and translational bubble dynamics. in *Bubble and Particle Dynamics in Acoustic Fields: Modern Trends and Applications* 95–143 (Research Signpost, 2005).
10. Lamb, H. *Hydrodynamics*. (Dover publications, 1945).
11. Plesset, Milton S.; Prosperetti, A. Bubble dynamics and cavitation. *Annu. Rev. Fluid Mech.* **9**, 85–145 (1977).
12. Leighton, T. G. *The Acoustic Bubble*. (Academic Press, 2012).
13. Yosioka, K., Kawasima, Y. & Hirano, H. Acoustic radiation pressure on bubbles and their logarithmic decrement. *Acta Acust. united with Acust.* **5**, 173-178(6) (1955).
14. Zabolotskaya, E. A. Interaction of gas bubbles in a sound field. *Sov. Phys. Acoust.* **30**, 365–368 (1984).
15. Boluriaan, S. & Morris, P. J. Acoustic Streaming: From Rayleigh to Today. *Int. J. Aeroacoustics* **2**, 255–292 (2003).
16. Eckart, C. Vortices and streams caused by sound waves. *Phys. Rev.* **73**, 68–76 (1948).
17. Nama, N., Huang, P. H., Huang, T. J. & Costanzo, F. Investigation of acoustic streaming patterns around oscillating sharp edges. *Lab Chip* **14**, 2824–2836 (2014).
18. Muller, P. B., Barnkob, R., Jensen, M. J. H. & Bruus, H. A numerical study of microparticle acoustophoresis driven by acoustic radiation forces and streaming-induced drag forces. *Lab Chip* **12**, 4617–4627 (2012).

19. Muller, P. B. & Bruus, H. Numerical study of thermoviscous effects in ultrasound-induced acoustic streaming in microchannels. *Phys. Rev. E - Stat. Nonlinear, Soft Matter Phys.* **90**, 043016 (2014).

20. Behdani, B., Monjezi, S., Zhang, J., Wang, C. & Park, J. Direct numerical simulation of microbubble streaming in a microfluidic device: The effect of the bubble protrusion depth on the vortex pattern. *Korean J. Chem. Eng.* **37**, 2117–2123 (2020).

21. Ovchinnikov, M., Zhou, J. & Yalamanchili, S. Acoustic streaming of a sharp edge. *J. Acoust. Soc. Am.* **136**, 22–29 (2014).

22. Zhang, C., Guo, X., Royon, L. & Brunet, P. Unveiling of the mechanisms of acoustic streaming induced by sharp edges. *Phys. Rev. E* **102**, 043110 (2020).

23. Doinikov, A. A., Gerlt, M. S., Pavlic, A. & Dual, J. Acoustic streaming produced by sharp-edge structures in microfluidic devices. *Microfluid. Nanofluidics* **24**, 32 (2020).

24. Kaynak, M. *et al.* Acoustic actuation of bioinspired microswimmers. *Lab Chip* **17**, 395–400 (2017).

25. Spelman, T. A. & Lauga, E. Arbitrary axisymmetric steady streaming: flow, force and propulsion. *J. Eng. Math.* **105**, 31–65 (2017).

26. Bertin, N. *et al.* Propulsion of Bubble-Based Acoustic Microswimmers. *Phys. Rev. Appl.* **4**, 064012 (2015).

27. Dolev, A., Kaynak, M. & Sakar, M. S. Dynamics of entrapped microbubbles with multiple openings. *Phys. Fluids* **34**, 012012 (2022).

28. Kaynak, M., Dolev, A. & Sakar, M. S. 3D Printed Acoustically Programmable Soft Microactuators. *Soft Robot.* (2022) doi:10.1089/soro.2021.0193.

29. Spelman, T. A., Stephan, O. & Marmottant, P. Multi-directional bubble generated streaming flows. *Ultrasonics* **102**, 106054 (2020).

30. Wu, J. Acoustical tweezers. *J. Acoust. Soc. Am.* **89**, 2140–2143 (1991).

31. Ozcelik, A. *et al.* Acoustic tweezers for the life sciences. *Nature Methods* vol. 15 1021–1028 (2018).

32. Ding, X. *et al.* On-chip manipulation of single microparticles, cells, and organisms using surface acoustic waves. *Proc. Natl. Acad. Sci. U. S. A.* **109**, 11105–11109 (2012).

33. Rayleigh, Lord. On waves propagated along the plane surface of an elastic solid. *Proc. London Math. Soc.* **s1-17**, 4–11 (1885).

34. Ahmed, D. *et al.* Rotational manipulation of single cells and organisms using acoustic waves. *Nat. Commun.* **7**, 1–11 (2016).

35. Ozcelik, A. *et al.* Acoustofluidic Rotational Manipulation of Cells and Organisms Using Oscillating Solid Structures. *Small* **12**, 5120–5125 (2016).

36. Bücks, K. & Müller, H. Über einige Beobachtungen an schwingenden Piezoquarzen und ihrem Schallfeld. *Zeitschrift für Phys.* **84**, 75–86 (1933).

37. Buchanan, R. H., Jameson, G. & Oedjoe, D. Cyclic migration of bubbles in vertically vibrating liquid columns. *Ind. Eng. Chem. Fundam.* **1**, 82–86 (1962).

38. Blake, F. G. Bjerknes Forces in Stationary Sound Fields. *J. Acoust. Soc. Am.* **21**, 551 (1949).

39. Vilhelm, B. *Fields of force*. (columbia university press, 1906).

40. Eller, A. Force on a Bubble in a Standing Acoustic Wave. *J. Acoust. Soc. Am.* **43**, 170–171 (1968).

41. Dolev, A., Davis, S. & Bucher, I. Noncontact Dynamic Oscillations of Acoustically Levitated Particles by Parametric Excitation. *Phys. Rev. Appl.* **12**, 034031 (2019).

42. Gu, Y. *et al.* Acoustofluidic centrifuge for nanoparticle enrichment and separation. *Sci. Adv.* **7**, (2021).

43. Lee, M. C. & Feng, I. A. Acoustic levitating apparatus for submillimeter samples. *Rev. Sci. Instrum.* **53**, 854–859 (1982).

44. Wu, J. & Du, G. Acoustic radiation force on a small compressible sphere in a focused beam. *J. Acoust. Soc. Am.* **87**, 997–1003 (1990).

45. Hertz, H. M. Standing-wave acoustic trap for nonintrusive positioning of microparticles. *J. Appl. Phys.* **78**, 4845–4849 (1995).

46. Silva, G. T. & Baggio, A. L. Designing single-beam multitrapping acoustical tweezers. *Ultrasonics* **56**, 449–455 (2015).

47. Lee, J. *et al.* Single beam acoustic trapping. *Appl. Phys. Lett.* **95**, 073701 (2009).

48. Lam, K. H. *et al.* Ultrahigh frequency lensless ultrasonic transducers for acoustic tweezers application. *Biotechnol. Bioeng.* **110**, 881–886 (2013).

49. Cannata, J. M., Ritter, T. A., Chen, W. H., Silverman, R. H. & Shung, K. K. Design of efficient, broadband single-element (20-80 MHz) ultrasonic transducers for medical imaging applications. *IEEE Trans. Ultrason. Ferroelectr. Freq. Control* **50**, 1548–1557 (2003).

50. Baresch, D., Thomas, J. L. & Marchiano, R. Observation of a Single-Beam Gradient Force Acoustical Trap for Elastic Particles: Acoustical Tweezers. *Phys. Rev. Lett.* **116**, 024301 (2016).

51. Marzo, A. *et al.* Holographic acoustic elements for manipulation of levitated objects. *Nat. Commun.* **6**, 1–7 (2015).

52. Li, J. *et al.* Three dimensional acoustic tweezers with vortex streaming. *Commun. Phys.* **4**, 1–8 (2021).

53. Courtney, C. R. P. *et al.* Dexterous manipulation of microparticles using Bessel-function acoustic pressure fields. *Appl. Phys. Lett.* **102**, 123508 (2013).

54. Seah, S., Drinkwater, B., Carter, T., Malkin, R. & Subramanian, S. Correspondence: Dexterous ultrasonic levitation of millimeter-sized objects in air. *IEEE Trans. Ultrason. Ferroelectr. Freq. Control* **61**, 1233–1236 (2014).

55. Melde, K. *et al.* Directed Acoustic Assembly in 3D. *arXiv Prepr.* (2022) doi:10.48550/arxiv.2210.07153.

56. Baudoin, M. *et al.* Spatially selective manipulation of cells with single-beam acoustical tweezers. *Nat. Commun.* **11**, (2020).

57. Baudoin, M. *et al.* Folding a focalized acoustical vortex on a flat holographic transducer: Miniaturized selective acoustical tweezers. *Sci. Adv.* **5**, (2019).

58. Baresch, D., Thomas, J. L. & Marchiano, R. Spherical vortex beams of high radial degree for enhanced single-beam tweezers. *J. Appl. Phys.* **113**, (2013).

59. Baudoin, M. & Thomas, J. L. Acoustic Tweezers for Particle and Fluid Micromanipulation. *Annual Review of Fluid Mechanics* vol. 52 205–234 (2020).

60. Dolev, A. Entrapped MicroBubble Dynamics. *MATLAB Central File Exchange* https://www.mathworks.com/matlabcentral/fileexchange/123075-entrapped-microbubble-dynamics (2023).

61. Louf, J. F., Bertin, N., Dollet, B., Stephan, O. & Marmottant, P. Hovering Microswimmers Exhibit Ultrafast Motion to Navigate under Acoustic Forces. *Adv. Mater. Interfaces* **5**, 1800425 (2018).

62. Feng, J., Yuan, J. & Cho, S. K. Micropropulsion by an acoustic bubble for navigating microfluidic spaces. *Lab Chip* **15**, 1554–1562 (2015).

63. Ahmed, D. *et al.* Selectively manipulable acoustic-powered microswimmers. *Sci. Rep.* **5**, (2015).

64. Ren, L. *et al.* 3D steerable, acoustically powered microswimmers for single-particle manipulation. *Sci. Adv.* **5**, eaax3084 (2019).

65. McNeill, J. M., Nama, N., Braxton, J. M. & Mallouk, T. E. Wafer-Scale Fabrication of Micro- To Nanoscale Bubble Swimmers and Their Fast Autonomous Propulsion by Ultrasound. *ACS Nano* **14**, 7520–7528 (2020).

66. Sridhar, V., Park, B. W. & Sitti, M. Light-Driven Janus Hollow Mesoporous TiO2–Au Microswimmers. *Adv. Funct. Mater.* **28**, 1704902 (2018).

67. Aghakhani, A., Yasa, O., Wrede, P. & Sitti, M. Acoustically powered surface-slipping mobile microrobots. *Proc. Natl. Acad. Sci. U. S. A.* **117**, 3469–3477 (2020).

68. Aghakhani, A. *et al.* High shear rate propulsion of acoustic microrobots in complex biological fluids. *Sci. Adv.* **8**, 5126 (2022).

69. Huang, P. H. *et al.* An acoustofluidic micromixer based on oscillating sidewall sharp-edges. *Lab Chip* **13**, 3847–3852 (2013).

70. Huang, P. H. *et al.* A reliable and programmable acoustofluidic pump powered by oscillating sharp-edge structures. *Lab Chip* **14**, 4319–4323 (2014).

71. Kaynak, M. *et al.* Acoustofluidic actuation of in situ fabricated microrotors. *Lab Chip* **16**, 3532–3537 (2016).

72. Kaynak, M., Ayhan, F. & Sakar, M. S. Compound micromachines powered by acoustic streaming. in *2019 International Conference on Robotics and Automation (ICRA)* 225–230 (IEEE, 2019). doi:10.1109/ICRA.2019.8793481.

73. Ahmed, D. *et al.* Artificial Swimmers Propelled by Acoustically Activated Flagella. *Nano Lett.* **16**, 4968–4974 (2016).

74. Liu, F. W. & Cho, S. K. 3-D swimming microdrone powered by acoustic bubbles. *Lab Chip* **21**, 355–364 (2021).

75. Kaynak, M., Dirix, P. & Sakar, M. S. Addressable Acoustic Actuation of 3D Printed Soft Robotic Microsystems. *Adv. Sci.* 2001120 (2020) doi:10.1002/advs.202001120.

76. Drinkwater, B. W. A Perspective on acoustical tweezers - Devices, forces, and biomedical applications. *Appl. Phys. Lett.* **117**, 180501 (2020).

77. Rufo, J., Zhang, P., Zhong, R., Lee, L. P. & Huang, T. J. A sound approach to advancing healthcare systems: the future of biomedical acoustics. *Nat. Commun.* **13**, (2022).

78. Ghanem, M. A. *et al.* Noninvasive acoustic manipulation of objects in a living body. *Proc. Natl. Acad. Sci. U. S. A.* **117**, 16848–16855 (2020).

79. Ozdas, M. S. *et al.* Non-invasive molecularly-specific millimeter-resolution manipulation of brain circuits by ultrasound-mediated aggregation and uncaging of drug carriers. *Nat. Commun.* **11**, (2020).

80. Lo, W. C., Fan, C. H., Ho, Y. J., Lin, C. W. & Yeh, C. K. Tornado-inspired acoustic vortex tweezer for trapping and manipulating microbubbles. *Proc. Natl. Acad. Sci. U. S. A.* **118**, (2021).

81. Baresch, D. & Garbin, V. Acoustic trapping of microbubbles in complex environments and controlled payload release. *Proc. Natl. Acad. Sci. U. S. A.* **117**, 15490–15496 (2020).

82. Jooss, V. M., Bolten, J. S., Huwyler, J. & Ahmed, D. In vivo acoustic manipulation of microparticles in zebrafish embryos. *Sci. Adv.* **8**, (2022).

83. Qiu, T. *et al.* Wireless Acoustic-Surface Actuators for Miniaturized Endoscopes. *ACS Appl. Mater. Interfaces* **9**, 42536–42543 (2017).

84. Ashkenazi, S., Huang, S. W., O'Donnell, M., Chao, C. Y. & Guo, L. J. High-frequency ultrasound transduction using polymer microring resonators. in *Proceedings - IEEE Ultrasonics Symposium* vol. 1 1056–1059 (2006).